The Journal of Immunology

Visualizing the Site and Dynamics of IgG Salvage by the MHC Class I-Related Receptor, FcRn

Raimund J. Ober, Cruz Martinez, Carlos Vaccaro, Jinchun Zhou and E. Sally Ward

J Immunol 2004; 172:2021-2029; ;
doi: 10.4049/jimmunol.172.4.2021
http://www.jimmunol.org/content/172/4/2021

The Journal of Immunology is published twice each month by
The American Association of Immunologists, Inc.,
9650 Rockville Pike, Bethesda, MD 20814-3994.

Print ISSN: 0022-1767 Online ISSN: 1550-6606.

Visualizing the Site and Dynamics of IgG Salvage by the MHC Class I-Related Receptor, FcRn[1]

Raimund J. Ober,* Cruz Martinez,† Carlos Vaccaro,† Jinchun Zhou,† and E. Sally Ward[2]*†

The MHC class I-related receptor, FcRn, plays a central role in regulating the serum levels of IgG. FcRn is expressed in endothelial cells, suggesting that these cells may be involved in maintaining IgG levels. We have used live cell imaging of FcRn-green fluorescent protein transfected human endothelial cells to analyze the intracellular events that control IgG homeostasis. We show that segregation of FcRn-IgG complexes from unbound IgG occurs in the sorting endosome. FcRn or FcRn-IgG complexes are gradually depleted from sorting endosomes to ultimately generate multivesicular bodies whose contents are destined for lysosomal degradation. In addition, the pathways taken by FcRn and the transferrin receptor overlap, despite distinct mechanisms of ligand uptake. The studies provide a dynamic view of the trafficking of FcRn and its ligand and have relevance to understanding how FcRn functions to maintain IgG homeostasis. ***The Journal of Immunology*****, 2004, 172: 2021–2029.**

Recent data indicate that in addition to its earlier known role in transferring maternal IgG from mother to young (1–4), the MHC class I-related receptor, FcRn, regulates the serum levels of IgG (5–7). Analyses in mice indicate that endothelial cells lining the (micro) vasculature are a possible site at which IgG homeostasis is maintained (8). Knowledge about how FcRn carries out its function in these cells is therefore of relevance to understanding how IgG levels are regulated and also to the effective delivery of therapeutic Abs.

FcRn expression in endothelial cells is primarily in intracellular organelles, with limited cell surface expression (5, 9). For nearly all FcRn species and IgG isotypes analyzed to date, the FcRn-IgG interaction is highly pH dependent, with binding occurring at pH 6.0 that becomes progressively weaker as neutral pH is approached (10–13). This pH dependence is mediated by the interaction of conserved IgG histidines located at the CH2-CH3 domain interface of the Fc region with acidic residues on FcRn (14–18). pH-dependent binding is consistent with the following model for FcRn function in endothelial cells (19): IgGs are taken up by FcRn-expressing cells and enter acidic endosomes where the FcRn-IgG interaction can occur. For several reasons, IgG uptake is believed to be via fluid phase pinocytosis rather than receptor mediated. First, limited, if any, surface FcRn expression can be detected (5, 9). Second, even if cell surface expression of FcRn occurs, the extracellular pH is generally not permissive for FcRn binding to IgG (10–13). FcRn is therefore unusual in that, unlike other receptors, in the majority of cell types it can only interact with ligand within acidic intracellular compartments after pinocytic uptake. Further, unlike many other serum components, the high concentrations of serum IgG (11–12 mg/ml for humans) (20) would be predicted to result in efficient uptake via this route. After uptake and binding to FcRn within acidic vesicles, IgGs are sorted, transported to the cell surface, and released at near neutral pH by poorly understood mechanisms. In contrast, IgGs that do not bind to FcRn after uptake into cells enter lysosomal compartments and undergo degradation (21). Lack of binding of an IgG to FcRn can be due to either low affinity or competition with other IgG molecules for interaction with a limited pool of FcRn. Consistent with this model, IgG/Fc fragments that have increased affinity for FcRn (while retaining pH-dependent binding) have a longer serum persistence (22).

Although models for FcRn function have been proposed (19, 23), there is a lack of knowledge concerning the intracellular pathways taken by FcRn and its IgG cargo. For example, no data are available concerning the site and dynamics of intracellular sorting events. Knowledge of these processes is central to understanding how IgG levels are controlled throughout the body. In this study we have used live cell fluorescence imaging of FcRn-green fluorescent protein (GFP)[3]-transfected endothelial cells to analyze in real time the trafficking of this receptor and its ligand. A custom-built, multiwavelength laser excitation microscope imaging system has been used in conjunction with an intensified camera to analyze the processes that regulate IgG homeostasis on a rapid time scale and for a larger number of acquisitions than could be achieved with a more standard imaging configuration. Our studies provide a dynamic view of the events that are involved in sorting FcRn-IgG complexes from uncomplexed IgG and identify the intracellular site at which these processes occur. They also show that the pathways taken by the transferrin receptor and FcRn within cells intersect, despite fundamentally different mechanisms of ligand uptake. These studies therefore provide novel insight into the pathways involved in IgG homeostasis.

Materials and Methods

Abs and reagents

Alexa 647-labeled dextran (M_r = 10 kDa; anionic, fixable), Alexa 546-labeled transferrin, and LysoTracker Red were obtained from Molecular

*Cancer Immunobiology Center and †Center for Immunology, University of Texas Southwestern Medical Center, Dallas, TX 75390

Received for publication September 4, 2003. Accepted for publication November 24, 2003.

The costs of publication of this article were defrayed in part by the payment of page charges. This article must therefore be hereby marked *advertisement* in accordance with 18 U.S.C. Section 1734 solely to indicate this fact.

[1] This work was supported by National Institutes of Health Grants RO1AI39167, RO1AI54707, and R21AI53748.

[2] Address correspondence and reprint requests to Dr. E. Sally Ward, Center for Immunology, NB9.106, University of Texas Southwestern Medical Center, 6000 Harry Hines Boulevard, Dallas, TX 75390-8576. E-mail address: sally.ward@utsouthwestern.edu

[3] Abbreviations used in this paper: GFP, green fluorescent protein; β_2m, human β_2-microglobulin; EEA1, early endosomal Ag-1; LAMP-1, lysosome-associated membrane glycoprotein-1.

0022-1767/04/$02.00

Probes (Eugene, OR). Unlabeled transferrin was obtained from Sigma-Aldrich (St. Louis, MO). Anti-early endosomal Ag-1 (anti-EEA1) and anti-GM130 Abs (both mouse IgG1) were obtained from BD Biosciences (Palo Alto, CA). Anti-lysosome-associated membrane glycoprotein-1 (anti-LAMP-1; mouse IgG1, clone H4A3 developed by Drs. T. August and J. Hildreth) was obtained from the Developmental Studies Hybridoma Bank developed under the auspices of the National Institute of Child Health and Human Development and maintained by the University of Iowa (Iowa City, IA). Alexa 568-labeled anti-mouse IgG (highly cross-adsorbed) was obtained from Molecular Probes. Human IgG1 (HuLys10) (24) and a mutated variant, His^{435} to alanine (H435A) (25), were purified using lysozyme-Sepharose as previously described (25). IgGs were labeled with Alexa 546 or Alexa 647 carboxylic acid (succimidyl ester; Molecular Probes) using the methods recommended by the manufacturer, except that the molar ratio of Alexa 546:IgG was 3:1 during the reaction (use of the recommended 10:1 ratio of Alexa 546 dye:IgG during labeling resulted in some nonspecific binding of the labeled IgG). Unincorporated fluorophore was removed by extensive dialysis. Labeled Abs were analyzed by surface plasmon resonance (21) to ensure that labeling had not affected their binding properties.

Plasmid constructs

The plasmid for the expression of human FcRn with C-terminally fused enhanced GFP was made using pEGFP-N1 (BD Biosciences, Palo Alto, CA) and has been described previously (26). A construct for the expression of human β_2-microglobulin (β_2m) was made by cloning the β_2m gene into pCB7, which is a hygromycin-resistant variant of pCB6 (27). The pCB7 was provided by Dr. M. Roth (University of Texas Southwestern Medical Center).

Cells and transfections

The human endothelial cell line HMEC-1.CDC (28), a dermal-derived microvasculature cell line, was provided by F. Candal (Centers for Disease Control, Atlanta, GA). These cells were maintained in phenol red-free Ham's F-12K medium (BioSource International, Camarillo, CA) before use in transfections. FCS was depleted of bovine IgG by passage over protein G-Sepharose. HMEC-1 cells were transiently transfected with FcRn-GFP and β_2m expression constructs (2–3 μg of each) using Nucleofector technology (Amaxa Biosystems, Cologne, Germany) and the protocol recommended for the transfection of human endothelial cells. Immediately after transfection, cells were plated in phenol red-free Ham's medium on MatTek dishes (35-mm, glass-bottom, microwell dishes; MatTek, Ashland, MA) for live cell imaging or on coverslips (size 1.5, 12 mm diameter; Fisher Scientific, Houston, TX) in a 24-well plate for immunofluorescence staining. Cells were used in experiments between 19–27 h post-transfection. Transfection with a GFP expression construct (pEGFP-N1) resulted in a diffuse location of GFP signal throughout the cell, indicating that the distribution of FcRn-GFP is specific for FcRn (data not shown).

Immunofluorescence studies of fixed cells

Transfected cells were fixed using 3.4% paraformaldehyde (20–30 min at room temperature) and were permeabilized using 0.05% saponin in PBS. Fixed/permeabilized cells were stained with 5 μg/ml anti-EEA1, 10 μg/ml anti-LAMP-1, or 5 μg/ml anti-GM130 Abs in 1% BSA in $DPBS^{2+}$ (PBS containing 1 mM $CaCl_2$, 0.5 mM $MgCl_2$, and 0.25 mM $MgSO_4$). After a 30-min incubation, cells were washed in $DPBS^{2+}$, and bound Ab was detected by incubation in 4 μg/ml Alexa 568-labeled anti-mouse IgG. Cells were washed, fixed, and mounted in Prolong (Molecular Probes). To analyze the distribution of Alexa 647-labeled IgG in cells, transfectants were incubated with 1 mg/ml IgG for 60 min in a 37°C, 5% CO_2 incubator. After the pulse period, cells were washed with $DPBS^{2+}$ and chased in prewarmed phenol red-free Ham's medium at 37°C for 60 min. Cells were washed, fixed, permeabilized, and stained with anti-LAMP-1, followed by Alexa 568-labeled anti-mouse IgG as described above.

Sample preparation for live cell imaging

Cells were pulsed with fluorescently labeled proteins or dextran in prewarmed, phenol red-free Ham's medium for 1 h at 37°C in a 5% CO_2 incubator at the following concentrations: Alexa 546-labeled IgGs at 0.5 or 1 mg/ml, Alexa 647-labeled dextran at 0.5 mg/ml, Alexa 546-labeled transferrin at 10–50 μg/ml. The dishes were then mounted onto an Axiovert microscope (Carl Zeiss, Thornwood, NY) and were heated through the objective to maintain a temperature of 37°C using a ΔT objective warmer (Bioptechs, Butler, PA). The cells were then washed five times with phenol red-free Ham's medium (prewarmed to 37°C) by adding 2–3 ml and rapidly removing medium via a vacuum line. After the final wash was complete, 1 ml of prewarmed Ham's medium was added. In some cases where cells were pulsed with labeled transferrin, 1 mg/ml unlabeled transferrin was added to the chase medium. When used, LysoTracker Red was added to the chase medium at 24 μg/ml. Cells were immediately imaged (1–2 min expired between the first wash and the start of data acquisition) for up to 40 min (in a minority of experiments for which data are not shown, images were collected for up to 60 min). For imaging of FcRn-GFP in transfected cells, the same procedure was followed, except that cells were not pulse-chased with fluorescently labeled material before imaging.

Image acquisition and processing

Images of fixed cells were acquired using a Zeiss (Axiovert 200M) inverted epifluorescent microscope fitted with a ×100 (1.4 NA) Plan Apo objective (Carl Zeiss) using a cooled CCD camera (Orca ER, Hamamatsu, Bridgewater, NJ). Standard fluorescent (HQ) filter sets for GFP, TRITC, and Cy5 were obtained from Chroma Technology (Brattleboro, VT). For live cell imaging, series of images were acquired using a Zeiss Axiovert 100TV inverted fluorescence microscope fitted with a ×100 (1.65 NA) apochromatic objective (Olympus, Melville, NY). A Zeiss ×1.6 Optovar was used to further increase magnification. Using a custom-built, right side-facing filter cube, three laser lines were used for wide-field excitation: a 488-nm laser (Laser Physics, West Jordan, UT), a 543-nm laser (Research Electro-Optics, Boulder, CO), and a 633-nm laser (JDS Uniphase, San Jose, CA). Custom filter sets and beam splitters were used (Chroma Technology) for combining the laser lines on a breadboard and guiding the emitted fluorescence to the camera. Images were acquired with an intensified CCD camera (IpentaMax; Roper Scientific, Trenton, NJ). Three acquisition configurations were used. In the first configuration, single-color images of cells were acquired using Winview 2.5 software (Roper Scientific, Trenton, NJ). The exposure time was the repetition rate, which ranged from 100–500 ms. In the second configuration, cells were imaged in two colors. Sequential images were acquired for each color by switching between laser lines with fast shutters (Uniblitz, Rochester, NY) and using a dual-band emission filter. The exposure time for each color was 500 ms, and each pair was acquired every 1.2 s. In the third configuration, cells were imaged in two and three colors. Sequential images were acquired for each color by switching between laser lines with fast shutters and placing the corresponding emission filter into position using an emission filter wheel (Ludl Electronic Products, Hawthorne, NY). The exposure time for each color was 500 ms, and a set of images was acquired every 4 s. For the second and third approaches, custom-written software was used to control the various hardware components. In all cases, background fluorescence levels obtained from untreated cells in medium at the exposure times used for each fluorophore were analyzed and were found to be negligible. In addition, emission bleed-through of one fluorophore into the emission for a distinct fluorophore was negligible.

All data were processed and displayed using a custom-written software package in the high level programming language Matlab (The Mathworks, Nantick, MA). If necessary, for overlay images of cells the intensities of the individual components were adjusted to similar levels. The final images were exported for presentation in Canvas 8. Image series (overlays and single color) were translated in MatLab into movie format and exported for presentation in QuickTime format.

Results

FcRn-GFP is expressed in intracellular vesicles and tubules in transfected endothelial cells

In the current study we have analyzed the intracellular localization and trafficking of FcRn and its IgG ligand in the human endothelial cell line HMEC-1.CDC (28). This cell line has been chosen because it is derived from skin microvasculature, which is believed to be a possible site for the regulation of serum IgG levels (8, 29). Cells were transfected with a human FcRn-GFP fusion construct together with a human β_2m construct to facilitate live cell imaging. The β_2m construct was used to minimize the possibility that the expression of this protein becomes limiting for assembly of FcRn α-chain-β_2m heterodimers in endothelial cells, which would result in functional abnormalities of FcRn (30, 31). The expression of FcRn-GFP is primarily intracellular (Fig. 1), and the distribution is similar to that seen previously for endogenous expression in untransfected endothelial cells (8, 9). Analysis of the distribution of

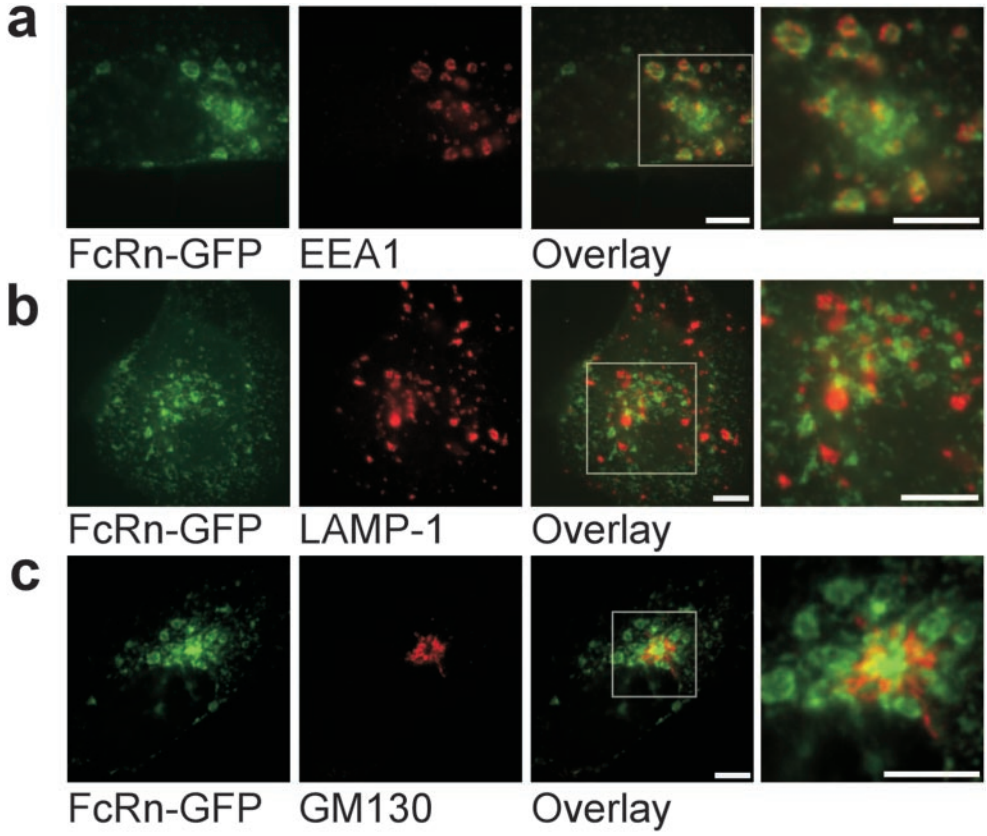

FIGURE 1. Analysis of distribution of FcRn in transfected HMEC-1 cells. FcRn-GFP-transfected HMEC-1 cells were fixed, permeabilized, and stained with anti-EEA1 (*a*), anti-LAMP-1 (*b*), or anti-GM130 (*c*). Bound primary Ab was detected using Alexa 568-labeled anti-mouse IgG. The *right panel* of *a–c* shows an expanded image of the overlay (boxed area). Images were acquired and processed as described in *Materials and Methods*. Data are representative of those obtained from at least five (anti-EEA1, anti-LAMP-1) or two (anti-GM130) independent experiments. Bar = 5 μm.

FcRn-GFP in transfected cells indicates that this receptor is expressed in EEA1-positive compartments, but not in LAMP-1-positive lysosomes (Fig. 1, *a* and *b*). Within these endosomes, of which the majority range in size from 1–2.5 μm, FcRn and EEA1 are generally distributed in discrete subdomains (Fig. 1*a*, *right panel*). Thus, although both FcRn and EEA1 codistribute within the same endosomes, their sublocalizations within these compartments appear to be distinct. In a high proportion of transfected cells, strong perinuclear staining was also observed and corresponded to Golgi expression (assessed using anti-GM130, a marker for the Golgi; Fig. 1*c*).

In addition to expression in 1- to 2.5-μm diameter endosomes, FcRn-GFP was present in tubules and smaller vesicles within the cells (Fig. 2). Live cell imaging was used to analyze the dynamics of FcRn movement on a rapid time scale (frames every 100 or 500 ms). In contrast to the larger, FcRn-expressing endosomes, which generally do not move over large distances in the cell, small, FcRn-positive vesicles and tubules are highly motile and show movement rates of up to 3 and 0.6 μm/s for vesicles and tubules, respectively (Fig. 2 and Web Movie 1 on the online supplementary information page[4]). Fusion of the vesicles and tubules with the endosomes can frequently be seen (Fig. 2 and Web Movie 1). In some cases, FcRn-positive tubules separate from one endosome before fusing with another (Fig. 2*b*).

FcRn-GFP is present in sorting endosomes

We first characterized the properties of the endosomes by pulsing cells with transferrin and dextran for 60 min. These markers are known to be sorted into the recycling (transferrin) and lysosomal pathways (dextran) in the sorting endosome. Their distribution was analyzed using live cell imaging for 7-min periods within a chase period of up to 20 min. Imaging was conducted using a custom-built, multiwavelength laser excitation imaging setup. This setup was designed to allow relatively rapid image acquisition for multiple fluorophores for large numbers of acquisitions. The use of laser excitation allowed wide bandpass emission filters to be employed to maximize the efficiency of collection of emission signal. In turn, this, in conjunction with the use of an intensified camera, resulted in the need for only low excitation power, reducing the undesirable loss of signal due to photobleaching. A complete set of images was acquired for the three fluorophores every 4 s. Transferrin can be seen in vesicles and tubules that extend from the endosomes, whereas dextran is located in the center of the compartment (Fig. 3). The tubules extend and in some cases separate from the endosome (not shown). Thus, these endosomes can be classified as sorting endosomes. In nearly all cases, FcRn-GFP in the sorting endosome is colocalized with transferrin, and transferrin-positive tubules also contain FcRn (Fig. 3). Therefore, at least during stages of trafficking that involve the sorting endosome, this FcR appears to follow the same pathway as the transferrin receptor.

Trafficking pathways of IgGs with different affinities for FcRn bifurcate in the sorting endosome

Having identified the sorting endosome in endothelial cells, we next analyzed whether this organelle is the site at which FcRn-IgG complexes are sorted from lysosomally destined IgG that is not bound to FcRn. Although IgGs that do not bind to FcRn have been shown to enter the lysosomal pathway (21), there is no knowledge

[4] The on-line version of this article contains supplemental material.

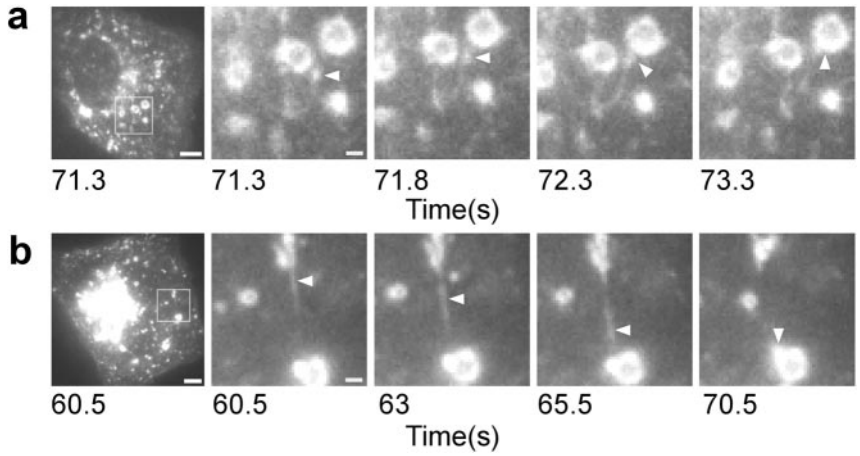

FIGURE 2. Tracking FcRn-GFP in transfected HMEC-1 cells. FcRn-GFP-transfected HMEC-1 cells were imaged at 37°C. The movement of FcRn-GFP was tracked with a fast image acquisition rate of 100 ms/frame (*a*) and a slower image acquisition rate of 500 ms/frame (*b*). The *left panels* of *a* and *b* show images of whole cells, with the boxed regions indicating the areas that were expanded in the adjacent panels. The arrows indicate areas of movement of FcRn-GFP-positive tubules or vesicles (times in seconds of frame relative to start of imaging are shown). These images are individual frames of movies, and Web Movie 1 that corresponds to the data shown in *a* can be viewed on the online supplementary information page. Images were acquired and processed as described in *Materials and Methods* (single-color configuration). Data show representative cells from at least six (*a*) or three (*b*) independent experiments. Bar = 5 μm (whole cell images) or 1 μm (expanded images).

of the processes and dynamics of the events that lead to sorting of FcRn-bound IgG away from free IgG. FcRn-GFP-transfected cells were therefore pulsed with fluorescently labeled IgGs that have different affinities for binding to FcRn: the wild-type human IgG1 molecule binds to FcRn, whereas a mutated variant (His^{435} to alanine, or H435A) does not interact with this receptor with a measurable affinity (25). This mutated IgG retains binding to FcγRs and to its Ag, hen egg lysosome, indicating that it is folded correctly (25). After a pulse of 60 min, labeled IgG was washed out, and live cell images of FcRn-GFP and Alexa 546-labeled IgG were collected. Dual-color, time-lapse experiments were conducted for up to 10-min (human IgG1, H435A mutant) or 20-min (H435A mutant) periods within a 20-min (human IgG1) or 40-min (H435A mutant) chase period after the washes. A complete set of images was acquired for the two fluorophores every 1.2 s for a total of up to 1000 two-color sets.

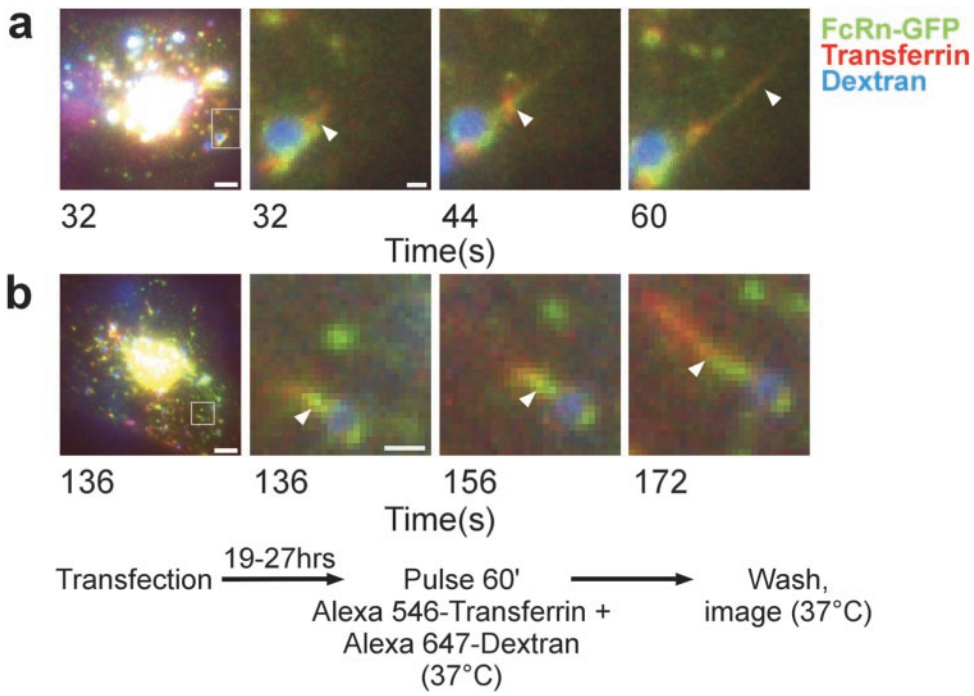

FIGURE 3. Trafficking of dextran and transferrin in FcRn-GFP-transfected HMEC-1 cells. *a* and *b*, FcRn-GFP-transfected HMEC-1 cells were pulsed for 60 min with 0.5 mg/ml Alexa 647-labeled dextran and 50 μg/ml Alexa 546-labeled transferrin, washed, and then imaged at 37°C. Individual frames from movies are shown. The *left panels* of *a* and *b* show images of whole cells, with boxed regions indicating the areas that were expanded in the adjacent panels. Times in seconds of frame relative to start of imaging are shown. For the images shown this was immediately after the beginning of the chase period. Arrowheads show FcRn-GFP- and transferrin-positive tubules extending from a dextran-positive endosome. Images were acquired and processed as described in *Materials and Methods* (filter wheel configuration). Representative cells from at least 21 independent experiments are shown. Bar = 5 μm (whole cell images) or 1 μm (expanded images).

At the concentrations of IgG used (0.5 or 1 mg/ml), human IgG1 is frequently colocalized with FcRn-GFP in small vesicles, tubules, and sorting endosomes (Fig. 4). However, some FcRn-GFP-positive compartments do not contain detectable levels of IgG1, and this is particularly marked for the sorting endosomes (Fig. 4*a*). This suggests that there may be trafficking hot spots within a cell to which internalized proteins (or other molecules) are directed. IgG1 can be seen in FcRn-GFP-positive tubules, which extend from the sorting endosome (Fig. 4, *b–d*, and Web Movie 2). These tubules are motile and can frequently be seen tethered to the sorting endosome, whereas in rarer cases the tubules detach and move at high speeds (~0.6 μm/s) through the cytosol (Fig. 4*c* and Web Movie 2). Frequently, the detached tubules move out of the focal plane or field of view, limiting the length of time for which they can be followed. In addition to detachment of tubules that contain FcRn-GFP and IgG1, smaller FcRn-GFP-positive, IgG1-positive vesicles (or possibly tubules) can also be seen leaving the sorting endosomes (Fig. 4*d*). The loss of FcRn-GFP-positive tubules and vesicles results in a progressive depletion of this receptor from the sorting endosome. Tubules attaching sorting endosomes to each other can also sometimes be observed, consistent with the sorting compartment being a continuous tubulo-vesicular network (Fig. 4*e*) (32, 33).

The behavior of the H435A mutant, which does not bind detectably to FcRn (25), is distinct from that of IgG1. This mutant accumulates in the vacuolar part of the sorting endosome and does not colocalize with FcRn-GFP (Fig. 5 and Web Movie 3). Similar to our observations with IgG1, the sorting endosomes within a cell show differences in the extent of IgG accumulation (Fig. 5, *b* and *d*). For IgG1-treated cells, FcRn-GFP-positive tubules are tethered and occasionally leave the sorting endosome (Fig. 5, *a–c*, and Web Movie 3). They also tether adjacent endosomes, and occasionally two endosomes with different amounts of labeled H435A fuse to mix their contents (Fig. 5*d*). However, and in contrast to human IgG1, labeled H435A mutant cannot be detected in the FcRn-GFP-positive tubules. FcRn-GFP is therefore gradually depleted from these compartments by loss of tubules and vesicles, and ultimately (after ~20–40 min) round, H435A-positive, FcRn-GFP-negative compartments remain (Fig. 5*e*). These compartments are generally characterized by higher mobility than their FcRn-GFP-positive progenitors and frequently move out of the focal plane or field of view (data not shown). To verify that the ultimate fate of the H435A mutant in these compartments is lysosomal, pulse-chase experiments were conducted under analogous conditions, but cells were fixed and stained with anti-LAMP-1 after a 60-min chase. Alexa 647-labeled H435A is extensively colocalized with LAMP-1 under these conditions (Fig. 5*f*).

The sorting endosomes mature to generate a multivesicular bodies

To further analyze the evolution of the sorting endosomes, LysoTracker Red was used. This fluorescently labeled weak base accumulates in acidic compartments (pH ~5.0 or below) and can

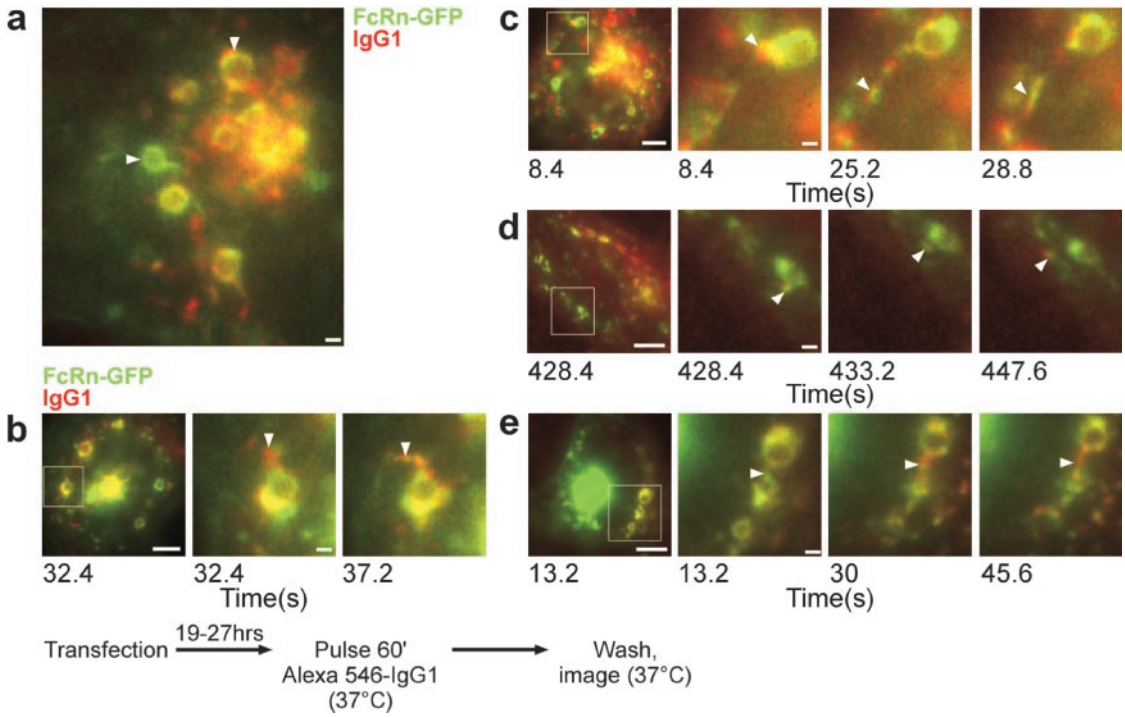

FIGURE 4. Trafficking of human IgG1 in FcRn-GFP-transfected HMEC-1 cells. Transfected cells were pulsed for 60 min with 0.5 mg/ml (*d* and *e*) or 1 mg/ml (*a–c*) Alexa 546-labeled IgG1. After the pulse, cells were washed and imaged at 37°C. Individual frames of movies are shown. The *left panels* of *b–e* show images of whole cells, with the boxed regions indicating the areas that were expanded in the adjacent panels. Times in seconds of each frame relative to start of imaging are shown; imaging was started at 0 s (*b* and *e*) or ~600 s (*c* and *d*) after the beginning of the chase period. The image in *a* was taken ~2 s after the beginning of an imaging period that immediately followed the start of the chase period. Arrowheads show the following: *a*, two FcRn-GFP-positive sorting endosomes within the same cell, which contain markedly different amounts of IgG1; *b*, an FcRn-GFP-positive, IgG1-positive tubule extending from a sorting endosome; *c*, an FcRn-GFP-positive, IgG1-positive tubule leaving a sorting endosome; *d*, an FcRn-GFP-positive, IgG1-positive vesicle leaving a sorting endosome; and *e*, FcRn-GFP-positive, IgG1-positive sorting endosomes tethered together by a tubule. Images were acquired and processed as described in *Materials and Methods* (dual-band emission filter configuration). Representative cells from at least 8 (*d* and *e*) and 34 (*a–c*) independent experiments are shown. Web Movie 2 (*c*) can also be viewed online. Bar = 1 μm (*a* and expanded images in *b–e*) or 5 μm (whole cell images in *b–e*).

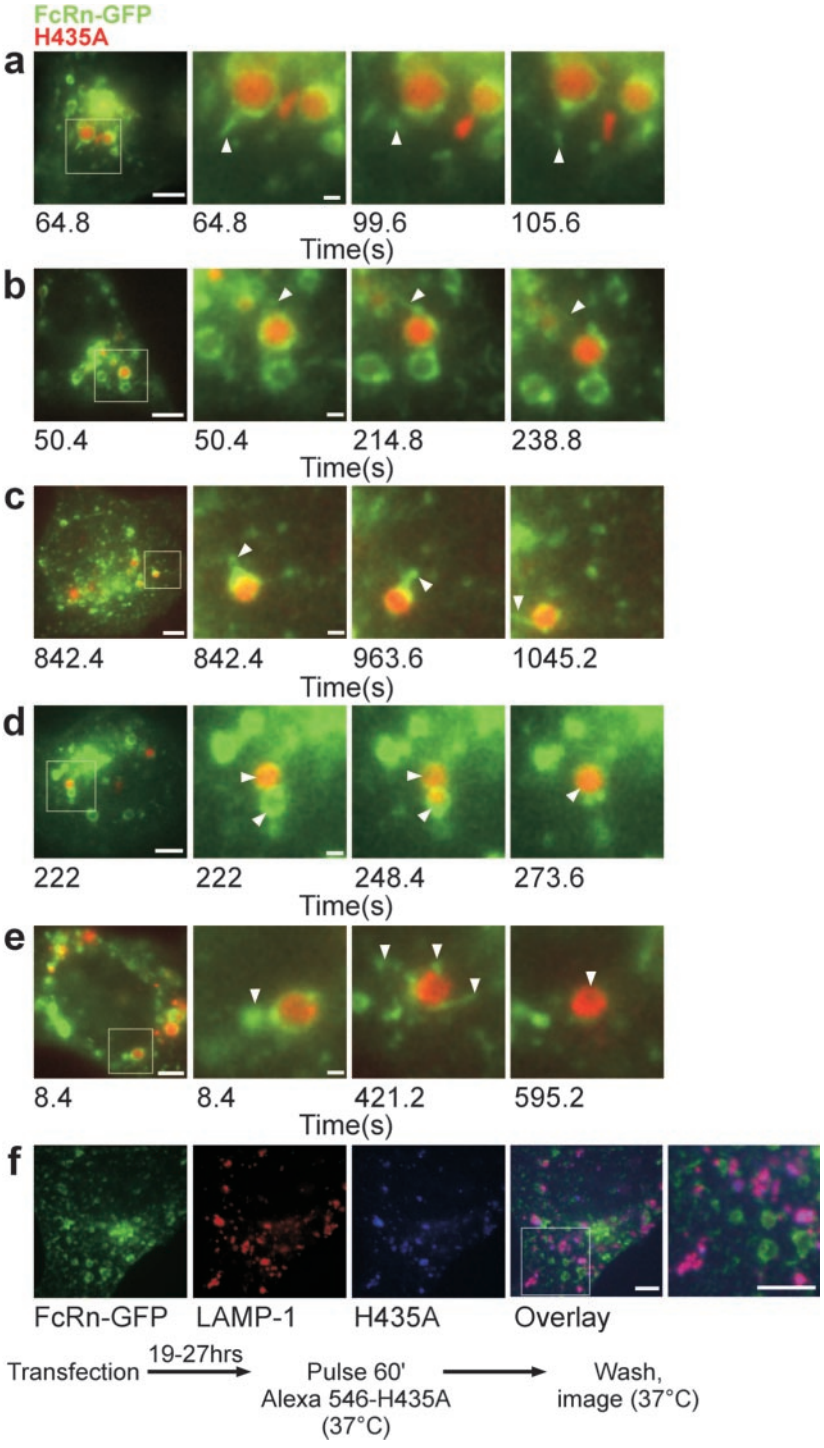

FIGURE 5. Trafficking of mutated human IgG1 (H435A) in FcRn-GFP-transfected HMEC-1 cells. Transfected cells were pulsed for 60 min with 1 mg/ml Alexa 546-labeled H435A. *a–e*, Live cell imaging was conducted at 37°C immediately after the pulse and washes. Individual frames of movies are shown. The *left panels* of *a–e* show images of whole cells, with the boxed regions indicating the areas that were expanded in the adjacent panels. Times in seconds of each frame relative to the start of imaging are shown; imaging was started at 0 s (*c*), ~600 s (*a* and *d*), or ~1200 s (*b* and *e*) after the beginning of the chase period. Arrowheads show the following: *a* and *b*, FcRn-GFP-positive tubules leaving an H435A-positive sorting endosome; *c*, FcRn-GFP-positive tubules tethered to an endosome containing H435A; *d*, merging of an FcRn-GFP, H435A positive endosome with an FcRn-GFP (no detectable H435A) endosome; and *e*, depletion of FcRn-GFP tubules from a sorting endosome to generate an H435A-positive, FcRn-GFP-negative compartment. For *a–e*, representative cells from at least 18 independent experiments are shown. *f*, Images of transfected cells pulsed with Alexa 647-labeled H435A followed by a 60-min chase and then fixation, permeabilization and staining with anti-LAMP-1. Bound anti-LAMP-1 was detected using Alexa 568-labeled anti-mouse IgG. The *right panel* in *f* shows an expansion of the overlay (boxed area). *f*, Data are representative of those obtained from at least three independent experiments. Live cell images (*a–e*) were acquired and processed as described in *Materials and Methods* (dual-band emission filter configuration). Web Movie 3 (*a*) can also be viewed online (see Footnote 4). Bar = 5 μm (whole cell images in *a–e* and both panels in *f*) or 1 μm (expanded images in *a–e*).

therefore be used to analyze late endosomal or lysosomal acidification. Addition of LysoTracker Red indicated that as FcRn-GFP-positive tubules were progressively shed from the sorting endosome, the intensity of LysoTracker Red signal increased (Fig. 6, *a* and *b*). Furthermore, in some cases, LysoTracker Red was confined to a subcompartment within the endosome, suggesting that internalization of membrane was occurring (Fig. 6*c*). These LysoTracker Red compartments therefore most likely represent maturing multivesicular bodies described in other systems (34–37).

Discussion

In the current study we have analyzed the trafficking of FcRn and its ligand, IgG, in human endothelial cells. Studies in mice suggest that FcRn expression in endothelial cells plays a role in regulating serum IgG levels (8), and the available data indicate a similar function in humans (21). In endothelial cells, FcRn is expressed primarily in intracellular vesicles, where it can bind to IgG in a highly pH-dependent way, with binding at pH 6.0 and release at pH 7.3 (12, 13). In contrast to the majority of other receptors (e.g., transferrin receptors), FcRn therefore functions at an intracellular, rather than cell surface, location and relies on fluid phase uptake for ligand delivery. In this study we have used live cell imaging with a custom-built microscope set up in conjunction with an intensified camera to analyze the intracellular events that discriminate IgGs that bind to FcRn from those that do not. This imaging set-up has allowed us to analyze the dynamics and the site of FcRn-mediated sorting in

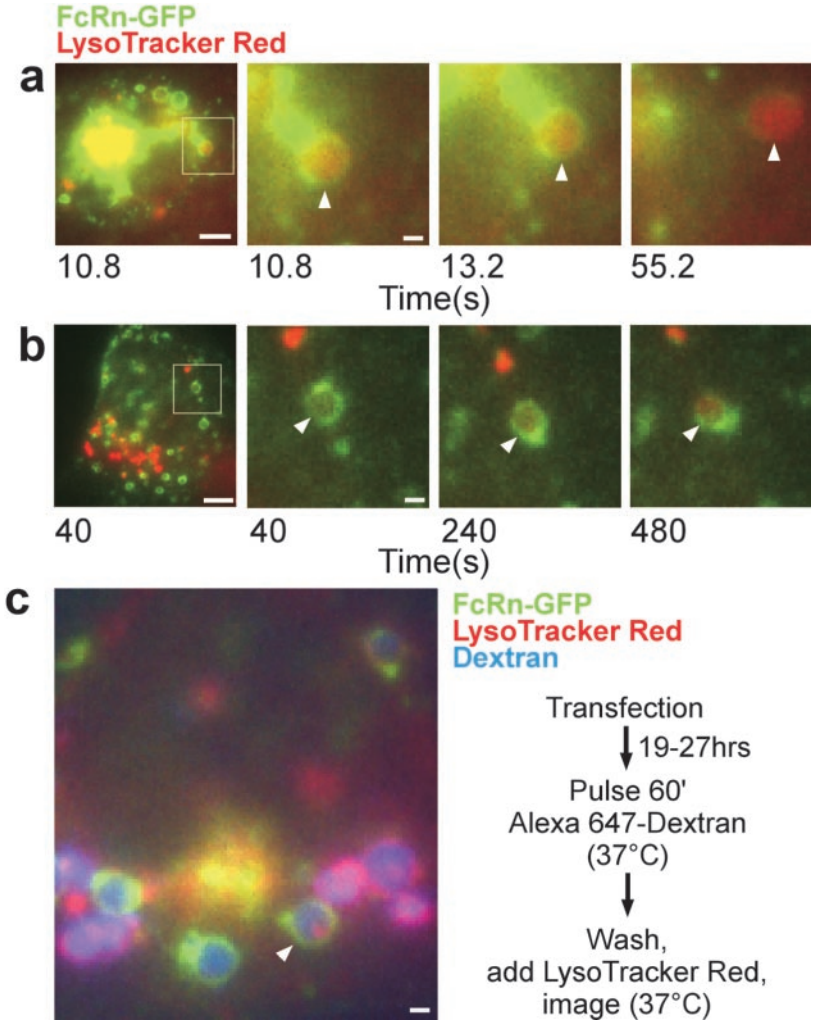

FIGURE 6. Trafficking of dextran and LysoTracker Red in FcRn-GFP-transfected HMEC-1 cells. Cells were incubated with 24 μg/ml LysoTracker Red (*a* and *b*) and imaged. *c*, Cells were first pulsed with 0.5 mg/ml Alexa 647-labeled dextran, washed, and incubated in 24 μg/ml LysoTracker Red. Individual frames are shown. The *left panels* of *a* and *b* show images of whole cells, with the boxed regions indicating the areas that were expanded in the adjacent panels. Times in seconds of each frame relative to start of imaging are shown; imaging was started at ~600 s (*a*) or ~1200 s (*b*) after the beginning of the chase period. The image in *c* was taken ~80 s after the beginning of an imaging period that immediately followed the start of the chase period. Arrowheads show the following: *a*, FcRn-GFP-positive, LysoTracker Red-positive endosome with gradual depletion of FcRn-GFP; *b*, FcRn-GFP-positive, LysoTracker Red-positive endosome showing an increase in LysoTracker Red fluorescence; and *c*, dextran-positive, FcRn-GFP-positive endosome in which only a subcompartment of the endosome is strongly LysoTracker Red positive, suggesting membrane internalization. Images were acquired and processed as described in *Materials and Methods* (both multicolor imaging configurations). Representative cells from at least eight (*a*), three (*b*), and nine (*c*) independent experiments are shown. Bar = 5 μm (whole cell images in *a* and *b*) or 1 μm (*c* and expanded images in *a* and *b*).

live cells and to demonstrate that the transferrin receptor and FcRn pathways intersect. Significantly, recent data have shown that FcRn plays a broad role not only in maintaining serum IgG homeostasis, but also in delivering IgG across epithelial cells to diverse body sites (38–42). Thus, knowledge of FcRn-mediated processes has relevance to understanding how IgG levels are regulated at diverse sites throughout the body.

The transfection of microvasculature-derived HMEC-1 cells with a FcRn-GFP construct results in FcRn-GFP expression throughout the cytosol in vesicles and tubules, with very limited cell surface expression. This distribution is consistent with earlier analyses of endogenous expression in endothelial cells, where punctate, vesicular staining throughout the cytosol was seen (8, 9). However, in these earlier studies the nature of the vesicles was not characterized. In this study we show that a high proportion of the FcRn-GFP-expressing compartments are also positive for the early endosomal marker, EEA1. Many of these endosomes have a size of 1–2.5 μm and, based on their handling of transferrin and dextran, have the properties of sorting endosomes. Endosomes of similar size have been described in other cell types after transfection with expression constructs for a GTPase-deficient form of the Rab5 GTPase, $Rab5^{Q79L}$, or rabaptin-GFP (43, 44). Significantly, in the current study the size of the endosomes is not a consequence of transfection, as they are also present in untransfected cells (data not shown), suggesting that this may be a general feature of endothelial cells. Within the sorting endosomes, FcRn-GFP and EEA1 are generally not colocalized and are seen in distinct subdomains. As EEA1 binds to Rab5 GTPase (45), which has been shown to form discrete subdomains in endosomes (46), this suggests that FcRn-GFP is associated with subdomains containing other effectors, such as Rab4 GTPase. This would be consistent with the proposed role of Rab4 in recycling, whereas Rab5 regulates endosome docking and fusion (46–48). The distribution of FcRn is distinct from that of LAMP-1, indicating that, consistent with its salvage function, it is not present in lysosomes.

Live cell imaging of FcRn-GFP on a rapid time scale indicates that FcRn-positive vesicles and tubules, with the exception of the sorting endosomes, are highly motile and can be propelled through the cytosol at speeds up to 3 μm/s. Fusion of these vesicles and tubules with the sorting endosomes can be visualized. By analyzing the trafficking of transferrin in FcRn-GFP-transfected cells, we observed that the pathways taken by FcRn and the transferrin receptor intersect. Thus, although IgG and transferrin are taken up by fluid phase and receptor-mediated mechanisms, respectively, their sorting occurs at the same intracellular site, i.e., in the sorting endosome.

The use of a custom-built multicolor laser excitation imaging system has allowed us to analyze the location and trafficking of FcRn and its IgG ligand in endothelial cells on a fast time scale for relatively long periods. This system is optimized for maximal collection of emission signal, thereby minimizing adverse effects due to photobleaching. Pulsing of cells with labeled human IgG1 followed by a chase has allowed us to visualize in real time the salvage of IgG away from the lysosomal route. Tubules positive

for both FcRn and IgG can be seen extending from the vacuole of the sorting endosome. Frequently, these tubules are tethered and can extend for large distances in the cytosol. Detachment of the tubules containing FcRn-GFP and IgG from the body of the sorting endosome can also be observed, and this is followed by rapid movement of the tubule and its disappearance. This loss of signal may be due to fusion of the tubule with the plasma membrane and rapid dispersal of the contents into (FcRn) and outside (IgG) the membrane. Alternatively, it may simply be due to movement of the tubule out of the focal plane or field of view. Similarly, less elongated vesicles containing FcRn and IgG also bud off the sorting endosomes. This results in a gradual depletion of FcRn-GFP and its IgG cargo from the sorting endosome.

A mutated variant of human IgG1 (H435A) that does not bind detectably to FcRn (25) follows a pathway distinct from that of its wild-type counterpart. This pathway is consistent with the short serum persistence of this Ab (25), which is retained by endothelial cells and ultimately colocalized with the lysosomal marker, LAMP-1. The H435A mutant accumulates in the vacuole of the sorting endosome and can rarely be seen in FcRn-positive tubules. Bifurcation of the pathways taken by human IgG1 and H435A after uptake into endothelial cells therefore occurs in the sorting endosome, and our images provide a dynamic view of the processes that occur to achieve this. In some cases complete loss of FcRn-GFP from the sorting endosome to leave a residual, IgG (H435A)-containing vesicle can be observed. Analyses with LysoTracker Red, a weak base-fluorophore conjugate that preferentially accumulates in acidic vesicles of pH 5.0 or less, indicate that acidification of the sorting endosomes to pH levels typical of late endosomes (or multivesicular bodies)/lysosomes (34) occurs while FcRn-positive tubules and vesicles are still being sorted. In some cases only a subcompartment of the vacuole is LysoTracker Red positive, which most likely is due to the extensive membrane internalization that characterizes multivesicular body formation (32, 49). Similarly, sorting of recycling receptors from lysosomally directed proteins in multivesicular bodies has been observed in other cell types, such as HEp-2 and NIH-3T3 cells (36, 49). Our data are consistent with maturation models of endosomal biogenesis in which (sorting) endosomes gradually mature into multivesicular bodies (34–37), rather than models in which endocytic carrier vesicles shuttle between early and late endosomes (50).

Endothelial cells are usually polarized with both apical and basolateral surfaces. In the current study we have analyzed transfected cells as subconfluent monolayers. It is probable that, as reported by others for epithelial cells (51), the endothelial cells have some polarized character when grown on glass. In contrast to epithelial cells (such as Madin-Darby canine kidney cells), for which extensive analyses of apical and basolateral endosomes and other intracellular compartments have been conducted (51–54), there is limited knowledge concerning intracellular trafficking in endothelial cells. Further studies will be necessary to determine which class of epithelial endosomes, if any, is analogous to the sorting endosomes analyzed in this study.

In summary, we have analyzed the dynamics and properties of trafficking of human FcRn in live endothelial cells. We have provided a dynamic view of the endosomal sorting of IgG that binds to FcRn into FcRn-positive tubules and vesicles. In contrast, IgG that does not interact with this FcR remains in the vacuole of the sorting endosome, which gradually matures into a multivesicular body. Our data show that the primary site at which FcRn sorts IgGs for either salvage or lysosomal degradation is the sorting endosome. In addition, the intracellular pathways taken by the transferrin receptor and FcRn overlap, although the mechanisms of ligand uptake for these two receptors are distinct. The analyses therefore provide new insight into the mechanism by which this receptor maintains IgG homeostasis.

Acknowledgments

We are indebted to Palmer Long for expert assistance with software development and the generation of the figures. We are grateful to Francisco Candal for generously providing us with the HMEC-1 cell line.

References

1. Rodewald, R., and J. P. Kraehenbuhl. 1984. Receptor-mediated transport of IgG. *J. Cell Biol. 99:159s.*
2. Simister, N. E., and A. R. Rees. 1985. Isolation and characterization of an Fc receptor from neonatal rat small intestine. *Eur. J. Immunol. 15:733.*
3. Roberts, D. M., M. Guenthert, and R. Rodewald. 1990. Isolation and characterization of the Fc receptor from the fetal yolk sac of the rat. *J. Cell Biol. 111:1867.*
4. Israel, E. J., V. K. Patel, S. F. Taylor, A. Marshak-Rothstein, and N. E. Simister. 1995. Requirement for a β_2-microglobulin-associated Fc receptor for acquisition of maternal IgG by fetal and neonatal mice. *J. Immunol. 154:6246.*
5. Ghetie, V., J. G. Hubbard, J. K. Kim, M. F. Tsen, Y. Lee, and E. S. Ward. 1996. Abnormally short serum half-lives of IgG in β_2-microglobulin-deficient mice. *Eur. J. Immunol. 26:690.*
6. Junghans, R. P., and C. L. Anderson. 1996. The protection receptor for IgG catabolism is the β_2-microglobulin-containing neonatal intestinal transport receptor. *Proc. Natl. Acad. Sci. USA 93:5512.*
7. Israel, E. J., D. F. Wilsker, K. C. Hayes, D. Schoenfeld, and N. E. Simister. 1996. Increased clearance of IgG in mice that lack β_2-microglobulin: possible protective role of FcRn. *Immunology 89:573.*
8. Borvak, J., J. Richardson, C. Medesan, F. Antohe, C. Radu, M. Simionescu, V. Ghetie, and E. S. Ward. 1998. Functional expression of the MHC class I-related receptor, FcRn, in endothelial cells of mice. *Int. Immunol. 10:1289.*
9. Antohe, F., L. Radulescu, A. Gafencu, V. Ghetie, and M. Simionescu. 2001. Expression of functionally active FcRn and the differentiated bidirectional transport of IgG in human placental endothelial cells. *Hum. Immunol. 62:93.*
10. Rodewald, R. 1976. pH-dependent binding of immunoglobulins to intestinal cells of the neonatal rat. *J. Cell Biol. 71:666.*
11. Wallace, K. H., and A. R. Rees. 1980. Studies on the immunoglobulin-G Fc-fragment receptor from neonatal rat small intestine. *Biochem. J. 188:9.*
12. Popov, S., J. G. Hubbard, J. Kim, B. Ober, V. Ghetie, and E. S. Ward. 1996. The stoichiometry and affinity of the interaction of murine Fc fragments with the MHC class I-related receptor, FcRn. *Mol. Immunol. 33:521.*
13. Raghavan, M., V. R. Bonagura, S. L. Morrison, and P. J. Bjorkman. 1995. Analysis of the pH dependence of the neonatal Fc receptor/immunoglobulin G interaction using antibody and receptor variants. *Biochemistry 34:14649.*
14. Kim, J. K., M. F. Tsen, V. Ghetie, and E. S. Ward. 1994. Localization of the site of the murine IgG1 molecule that is involved in binding to the murine intestinal Fc receptor. *Eur. J. Immunol. 24:2429.*
15. Medesan, C., D. Matesoi, C. Radu, V. Ghetie, and E. S. Ward. 1997. Delineation of the amino acid residues involved in transcytosis and catabolism of mouse IgG1. *J. Immunol. 158:2211.*
16. Kim, J. K., M. Firan, C. G. Radu, C. H. Kim, V. Ghetie, and E. S. Ward. 1999. Mapping the site on human IgG for binding of the MHC class I-related receptor, FcRn. *Eur. J. Immunol. 29:2819.*
17. Vaughn, D. E., C. M. Milburn, D. M. Penny, W. L. Martin, J. L. Johnson, and P. J. Bjorkman. 1997. Identification of critical IgG binding epitopes on the neonatal Fc receptor. *J. Mol. Biol. 274:597.*
18. Martin, W. L., A. P. J. West, L. Gan, and P. J. Bjorkman. 2001. Crystal structure at 2.8 Å of an FcRn/heterodimeric Fc complex: mechanism of pH dependent binding. *Mol. Cell. 7:867.*
19. Ghetie, V., and E. S. Ward. 2000. Multiple roles for the major histocompatibility complex class I-related receptor FcRn. *Annu. Rev. Immunol. 18:739.*
20. Waldmann, T. A., and W. Strober. 1969. Metabolism of immunoglobulins. *Prog. Allergy 13:1.*
21. Ward, E. S., J. Zhou, V. Ghetie, and R. J. Ober. 2003. Evidence to support the cellular mechanism involved in serum IgG homeostasis in humans. *Int. Immunol. 15:187.*
22. Ghetie, V., S. Popov, J. Borvak, C. Radu, D. Matesoi, C. Medesan, R. J. Ober, and E. S. Ward. 1997. Increasing the serum persistence of an IgG fragment by random mutagenesis. *Nat. Biotechnol. 15:637.*
23. Rojas, R., and G. Apodaca. 2002. Immunoglobulin transport across polarized epithelial cells. *Nat. Rev. Mol. Cell Biol. 3:944.*
24. Foote, J., and G. Winter. 1992. Antibody framework residues affecting the conformation of the hypervariable loops. *J. Mol. Biol. 224:487.*
25. Firan, M., R. Bawdon, C. Radu, R. J. Ober, D. Eaken, F. Antohe, V. Ghetie, and E. S. Ward. 2001. The MHC class I related receptor, FcRn, plays an essential role in the maternofetal transfer of gammaglobulin in humans. *Int. Immunol. 13:993.*
26. Ober, R. J., C. G. Radu, V. Ghetie, and E. S. Ward. 2001. Differences in promiscuity for antibody-FcRn interactions across species: implications for therapeutic antibodies. *Int. Immunol. 13:1551.*
27. Brewer, C. B. 1994. Cytomegalovirus plasmid vectors for permanent lines of polarized epithelial cells. *Methods Cell. Biol. 43:233.*
28. Pruckler, J. M., T. J. Lawley, and E. W. Ades. 1993. Use of a human microvascular endothelial cell line as a model system to evaluate cholesterol uptake. *Pathobiology 61:283.*

29. Junghans, R. P. 1997. Finally! The Brambell receptor (FcRB): mediator of transmission of immunity and protection from catabolism for IgG. *Immunol. Res. 16:29*.
30. Claypool, S. M., B. L. Dickinson, M. Yoshida, W. I. Lencer, and R. S. Blumberg. 2002. Functional reconstitution of human FcRn in Madin-Darby canine kidney cells requires co-expressed human β_2-microglobulin. *J. Biol. Chem. 277:28038*.
31. Praetor, A., and W. Hunziker. 2002. β_2-Microglobulin is important for cell surface expression and pH-dependent IgG binding of human FcRn. *J. Cell Sci. 115:2389*.
32. Hopkins, C. R., A. Gibson, M. Shipman, and K. Miller. 1990. Movement of internalized ligand-receptor complexes along a continuous endosomal reticulum. *Nature 346:335*.
33. Tooze, J., and M. Hollinshead. 1991. Tubular early endosomal networks in AtT20 and other cells. *J. Cell Biol. 115:635*.
34. Murphy, R. F. 1991. Maturation models for endosome and lysosome biogenesis. *Trends Cell Biol. 1:77*.
35. van Deurs, B., P. K. Holm, L. Kayser, K. Sandvig, and S. H. Hansen. 1993. Multivesicular bodies in HEp-2 cells are maturing endosomes. *Eur. J. Cell Biol. 61:208*.
36. Futter, C. E., A. Pearse, L. J. Hewlett, and C. R. Hopkins. 1996. Multivesicular endosomes containing internalized EGF-EGF receptor complexes mature and then fuse directly with lysosomes. *J. Cell Biol. 132:1011*.
37. Luzio, J. P., B. M. Mullock, P. R. Pryor, M. R. Lindsay, D. E. James, and R. C. Piper. 2001. Relationship between endosomes and lysosomes. *Biochem. Soc. Trans. 29:476*.
38. Israel, E. J., S. Taylor, Z. Wu, E. Mizoguchi, R. S. Blumberg, A. Bhan, and N. E. Simister. 1997. Expression of the neonatal Fc receptor, FcRn, on human intestinal epithelial cells. *Immunology 92:69*.
39. Dickinson, B. L., K. Badizadegan, Z. Wu, J. C. Ahouse, X. Zhu, N. E. Simister, R. S. Blumberg, and W. I. Lencer. 1999. Bidirectional FcRn-dependent IgG transport in a polarized human intestinal epithelial cell line. *J. Clin. Invest. 104:903*.
40. Kobayashi, N., Y. Suzuki, T. Tsuge, K. Okumura, C. Ra, and Y. Tomino. 2002. FcRn-mediated transcytosis of immunoglobulin G in human renal proximal tubular epithelial cells. *Am. J. Physiol Renal Physiol. 282:F358.*
41. Haymann, J. P., J. P. Levraud, S. Bouet, V. Kappes, J. Hagege, G. Nguyen, Y. Xu, E. Rondeau, and J. D. Sraer. 2000. Characterization and localization of the neonatal Fc receptor in adult human kidney. *J. Am. Soc. Nephrol. 11:632*.
42. Spiekermann, G. M., P. W. Finn, E. S. Ward, J. Dumont, B. L. Dickinson, R. S. Blumberg, and W. I. Lencer. 2002. Receptor-mediated immunoglobulin G transport across mucosal barriers in adult life: functional expression of FcRn in the mammalian lung. *J. Exp. Med. 196:303*.
43. Stenmark, H., R. G. Parton, O. Steele-Mortimer, A. Lutcke, J. Gruenberg, and M. Zerial. 1994. Inhibition of rab5 GTPase activity stimulates membrane fusion in endocytosis. *EMBO J. 13:1287*.
44. Mattera, R., C. N. Arighi, R. Lodge, M. Zerial, and J. S. Bonifacino. 2003. Divalent interaction of the GGAs with the rabaptin-5-rabex-5 complex. *EMBO J. 22:78*.
45. Christoforidis, S., H. M. McBride, R. D. Burgoyne, and M. Zerial. 1999. The Rab5 effector EEA1 is a core component of endosome docking. *Nature 397:621*.
46. Sonnichsen, B., S. De Renzis, E. Nielsen, J. Rietdorf, and M. Zerial. 2000. Distinct membrane domains on endosomes in the recycling pathway visualized by multicolor imaging of Rab4, Rab5, and Rab11. *J. Cell Biol. 149:901*.
47. De Renzis, S., B. Sonnichsen, and M. Zerial. 2002. Divalent Rab effectors regulate the sub-compartmental organization and sorting of early endosomes. *Nat. Cell. Biol. 4:124*.
48. Miaczynska, M., and M. Zerial. 2002. Mosaic organization of the endocytic pathway. *Exp. Cell Res. 272:8*.
49. Felder, S., K. Miller, G. Moehren, A. Ullrich, J. Schlessinger, and C. R. Hopkins. 1990. Kinase activity controls the sorting of the epidermal growth factor receptor within the multivesicular body. *Cell 61:623*.
50. Cavalli, V., M. Corti, and J. Gruenberg. 2001. Endocytosis and signaling cascades: a close encounter. *FEBS Lett. 498:190*.
51. Brown, P. S., E. Wang, B. Aroeti, S. J. Chapin, K. E. Mostov, and K. W. Dunn. 2000. Definition of distinct compartments in polarized Madin-Darby canine kidney (MDCK) cells for membrane-volume sorting, polarized sorting and apical recycling. *Traffic 1:124*.
52. Odorizzi, G., A. Pearse, D. Domingo, I. S. Trowbridge, and C. R. Hopkins. 1996. Apical and basolateral endosomes of MDCK cells are interconnected and contain a polarized sorting mechanism. *J. Cell Biol. 135:139*.
53. Wang, E., P. S. Brown, B. Aroeti, S. J. Chapin, K. E. Mostov, and K. W. Dunn. 2000. Apical and basolateral endocytic pathways of MDCK cells meet in acidic common endosomes distinct from a nearly-neutral apical recycling endosome. *Traffic 1:480*.
54. Leung, S. M., W. G. Ruiz, and G. Apodaca. 2000. Sorting of membrane and fluid at the apical pole of polarized Madin-Darby canine kidney cells. *Mol. Biol. Cell 11:2131*.